Engineering Structures 325 (2025) 119441

Contents lists available at ScienceDirect

Engineering Structures

journal homepage: www.elsevier.com/locate/engstruct

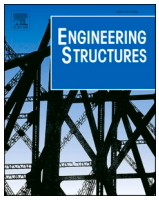

Performance and robustness assessment of roadway masonry arch bridges to scour-induced damage using multiple traffic load models

Prateek Kumar Dhir [a], Daniele Losanno [a], Enrico Tubaldi [b], Fulvio Parisi [a,*]

[a] Department of Structures for Engineering and Architecture, University of Naples Federico II, Italy
[b] Department of Civil and Environmental Engineering, University of Strathclyde, Glasgow, UK

ARTICLE INFO

Keywords:
Masonry arch bridges
Scour
Traffic loading
Robustness
Finite element macro-modelling

ABSTRACT

Masonry arch bridges are highly vulnerable to floods and particularly to scour, as demonstrated by the many collapses that regularly occur in Europe. Scour levels that do not directly cause the collapse of a bridge may result in a significant reduction of their capability to withstand traffic loading. Thus, research on the performance of masonry arch bridges under combined scour and traffic loading, and their structural robustness, is of paramount importance. This study evaluates the behaviour of masonry arch bridges subjected to scour and traffic loading by analysing a representative case study with a three-dimensional finite element model developed in Abaqus according to a macro-modelling approach. Traffic load is selected in accordance with different code-based models, including those provided by Italian guidelines for safety assessment of existing bridges. The scouring process is imposed through the progressive removal of elements at the foundation level. Displacements and internal stress distributions for different bridge components are recorded and the capacity of the masonry bridge is estimated under increasing traffic load for different scour levels. Results are obtained in terms of both local and global response parameters to provide useful information on threshold levels for bridge safety and monitoring. The sensitivity of the bridge structural performance to material properties and traffic load position is also assessed. The study results can be useful to inform the decisions to be taken by bridge stakeholders (e.g. close bridge, limit traffic, keep bridge open) based on scour and/or structural response measurements.

1. Introduction

Bridges are critical components of road and railway networks that are exposed to multiple hazards [1], whose failure can have significant impact on the network functionality. Natural hazards, such as earthquakes, wind, floods, or extreme temperatures, threaten the safety and continued operation of bridges [2]. These hazards are expected to intensify in the near future due to changes in global climate [3–5]. The increase of traffic loading and the problem of overloading are also a major threat to bridge safety, particularly if combined with the fact that many existing bridges have been designed for lower traffic loads than the current ones and have experienced degradation over the years. In Italy, after the Polcevera bridge collapse in Genoa in 2018, public attention to structural safety of existing bridges has increased significantly, leading to the enforcement of new guidelines [6] for risk-based classification, safety checks and monitoring of existing bridges in 2020 [7,8]. Among the various novelties, the guidelines have introduced a multi-hazard risk assessment methodology where both hydraulic and traffic related hazards are considered, providing new traffic load models based on actual vehicles for safety checks of existing bridges [8].

Masonry arch bridges still constitute a significant proportion of the bridge stock in Europe and worldwide [9]. These bridges require significant attention by transport operators due to their socio-economic, cultural, and historical importance, and the fact that they have been exposed to degradation over the years. Masonry arch bridges crossing waterways are particularly vulnerable to scour because they are quite stiff structures built on shallow foundations or on timber piles that have rotten over the years [10].

Extensive research has been conducted in last decades to evaluate the complex behaviour of masonry arch bridges and their capacity against critical actions capable to induce collapse. Advanced three-dimensional models have been developed to evaluate the vertical load carrying capacity of these bridges, by accounting for the contribution of the various components, namely the piers, arches, backfill, abutments and spandrel walls (see e.g. [11–20]). Numerical strategies have also been proposed to evaluate the effects of scour on masonry arch bridges and describe the

* Corresponding author.
E-mail address: fulvio.parisi@unina.it (F. Parisi).

https://doi.org/10.1016/j.engstruct.2024.119441
Received 31 May 2024; Received in revised form 9 November 2024; Accepted 2 December 2024
Available online 10 December 2024

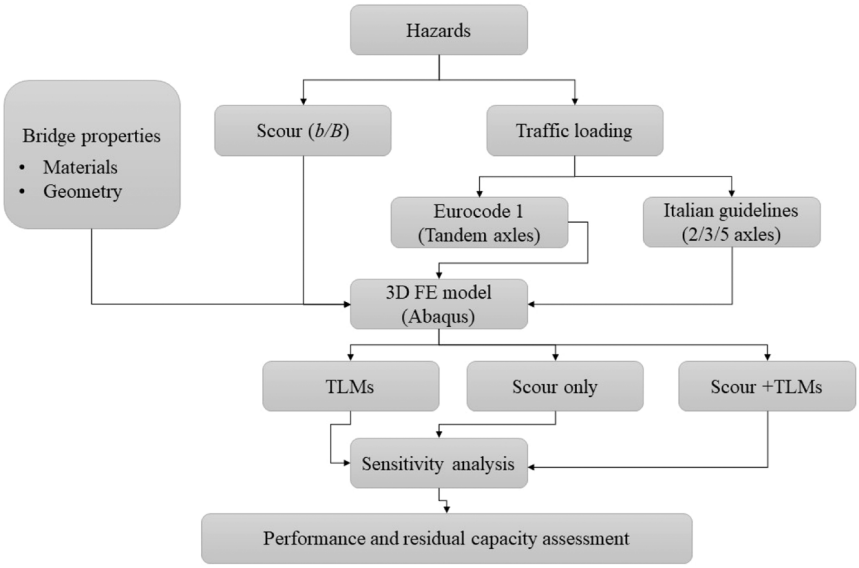

Fig. 1. Proposed framework for structural assessment of masonry arch bridges under scour and traffic loading.

Fig. 2. Nith bridge, New Cumnock (Scotland).

mechanisms leading to the collapse of real bridges [11,21–25]. To the best of the authors' knowledge, no research to date has considered the effect of the combined action of scour and traffic loading on masonry arch bridges. However, a study on this topic is of paramount importance given the fact that the presence of scour at the foundation level of masonry arch bridges may be unnoticed until severe levels occur, such that the foundation base is significantly undermined, and the bridge is close to collapse [11,26]. As a result of this, vehicles may be allowed to transit over a bridge during or at the end of a flood, with the combination of scour and traffic action leading to the bridge collapse and catastrophic consequences in terms of human losses [27]. It should be also noted that the management of existing masonry arch bridges should take into account their structural robustness to local damage, in order to ensure collapse prevention and life safety. While a huge number of studies have been carried out on progressive collapse and robustness of buildings (see e.g. [28]), structural robustness of existing bridges has been evaluated in few investigations [29–41], particularly on structural systems other than masonry arch bridges. This further calls for a study on robustness of masonry arch bridges against local damage, such as progressive loss of support produced by scour at the base of piers.

The main objective of this study is to develop a framework for performance and robustness assessment of roadway masonry arch bridges exposed to the multi-hazard combination of scour and traffic loading based on detailed numerical 3D modelling. The study also aims at identifying both the scour and traffic load-induced failure modes as well as their combined effects, providing relevant capacity curves and interaction domains. In this regard, this study can benefit the network operators and infrastructure owners to identify specific scour thresholds that call for traffic limitations to prevent bridge collapse.

The proposed procedure is comprehensively applied to assess the structural performance of a case study with geometrical properties consistent with a three-span masonry arch bridge over the Nith river, Scotland [42]. The bridge is investigated through a 3D finite element model (FEM) developed in Abaqus according to a macro-modelling approach. The scouring process is described by a progressive removal of cohesive elements under the foundation of the model representing in a simplified way the soil-structure interaction, and the bridge response – both in terms of traffic load-bearing capacity and damage mechanism – is evaluated accordingly. The role played by the uncertainty in key model parameters is also investigated by performing a sensitivity analysis. The results of this study provide useful information on the residual capacity to traffic loads of masonry arch bridges under increasing scour levels. Thus, the study outputs can be of interest to bridge managers, which have the challenging task to limit or even close the bridge to traffic during and after heavy floods based on limited information from visual inspections or assisted by sensors monitoring scour and/or the structural response. The study outcomes can also be useful for interpreting the failure mechanisms of previously collapsed bridges due to scour and traffic loading.

2. Methodology

This section illustrates the strategy developed to evaluate the performance and residual capacity of masonry bridges subjected to combined scour and traffic loading. The flowchart of the presented methodology for different load patterns and analysis types is shown in Fig. 1.

The methodology relies on the development of a FEM of the bridge, built in Abaqus using a macro-modelling approach, described in Section 3, and accounting for the behaviour of the various components of the bridge, including foundations, piers, abutments, arches, spandrels and backfill. In Section 4, the bridge model is analysed under the effect of gravity loads and traffic loads only, by carrying out nonlinear static analyses with different traffic load locations and magnification factors up to collapse. A parametric analysis is performed to investigate the sensitivity of the bridge capacity to the control strategy (i.e., displacement and forced control method), the vertical stiffness of the subgrade, the cohesion of the backfill, and the position of the traffic load model

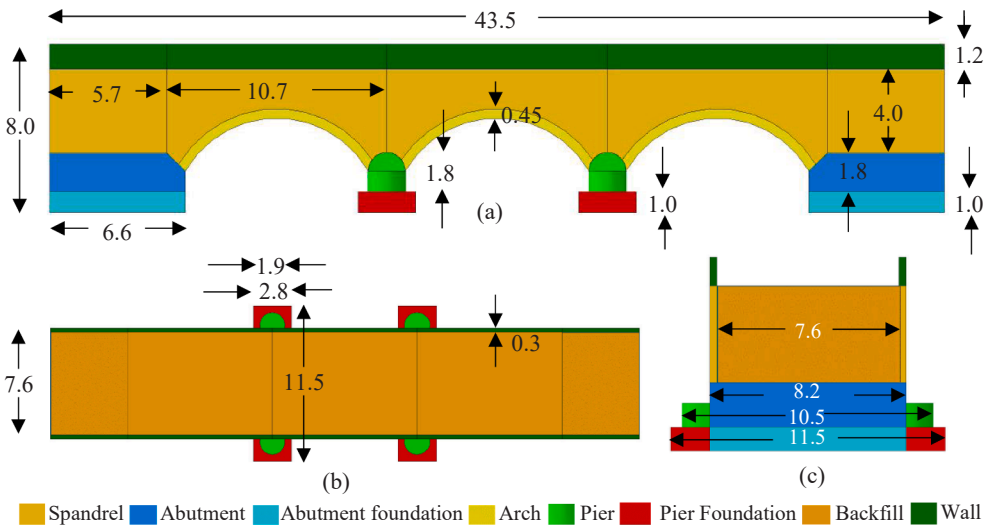

Fig. 3. Geometrical details of Nith bridge; (a) lateral/side view, (b) top view, and (c) cross section at abutment (units are in meters).

Table 1
Mechanical properties of materials and backfill-masonry contact interfaces.

Material/Surface	E [MPa]	σ_{c0} [MPa]	σ_{cu} [MPa]	σ_{t0} [MPa]	g_f [MPa·mm]	ϕ [-]	c_b [kPa]	μ[-]	k_n [N/mm^3]	k_t, k_s [N/mm^3]
Masonry (arches & spandrels)	3100	3.87	6.5	0.1	0.005	–	–	–	–	–
Masonry (piers)	2900	3.87	6.5	0.1	0.005	–	–	–	–	–
Masonry (abutment)	3000	3.87	6.5	0.1	0.005	–	–	–	–	–
Backfill	250	–	–	–	–	60°	10	–	–	–
Backfill-masonry contact Interfaces	–		–	–	–	–	–	0.6	500	500
Interactions between adjacent bridge components	–		–	–	–	–	–	0.6	500	500

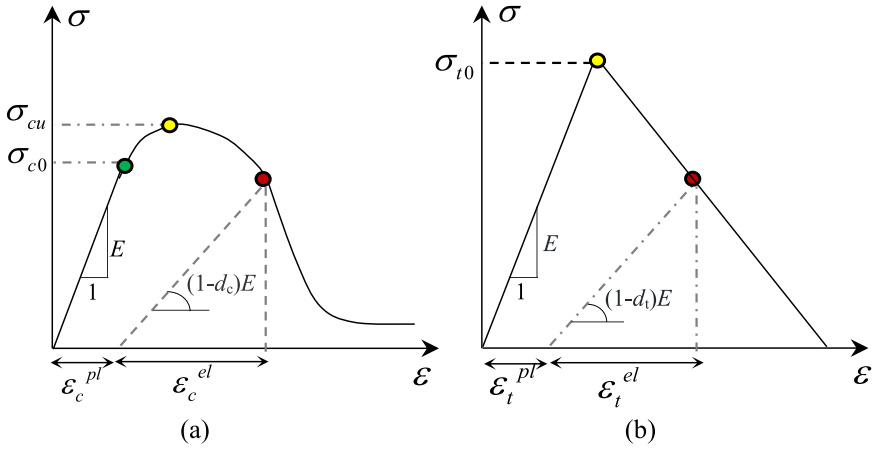

Fig. 4. Behaviour of CDP model considered in the analyses: (a) compression, and (b) tension.

(TLM). In Section 5, the bridge is subjected to gravity loads and scouring at the base of one of the piers, by increasing levels of scour up to collapse. Finally, in Section 6 the combined effects of scour and traffic loads are considered, by first performing an analysis for various levels of scour depth, and then by applying a TLM with increasing amplitudes. The residual capacity to withstand different TLMs for various scour scenarios is investigated.

3. Case study

3.1. Bridge geometrical properties

The case-study bridge is a three-span masonry arch bridge whose geometry is representative of many bridges built in Europe in the 19th century, such as the masonry bridge over the Nith river, in New Cumnock, Scotland (see Fig. 2). Fig. 3 illustrates the geometry of the case study, which is based on the bridge over the Nith river.

The total length and height of the bridge structure are equal to 43.5 m and 8 m, respectively. The width of the bridge superstructure is 8.2 m, with three shallow arches with span length and thickness equal to 10.7 m and 0.45 m, respectively. The two piers located in Nith river are 10.5-m-long, with both height and width equal to 1.8 m. The pier foundations are 11.5-m-long and 2.8-m-wide. The bridge abutments are characterised by length and height equal to 6.6 m and 2.8 m, respectively.

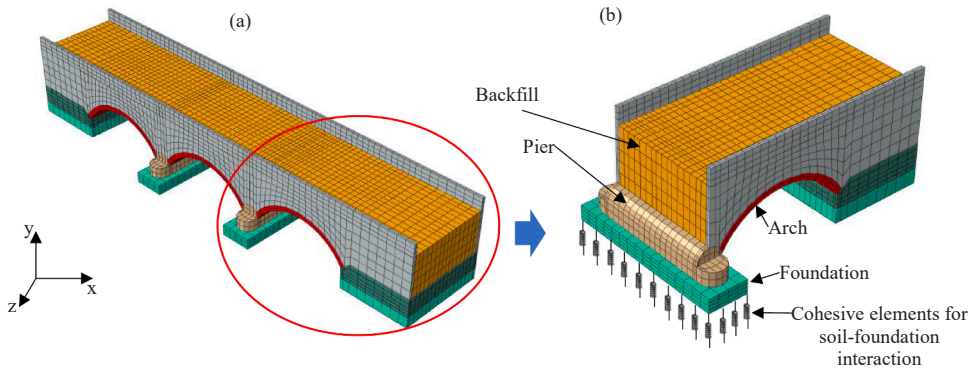

Fig. 5. (a) Meshed model, and (b) cohesive elements at the base of the pier foundation.

3.2. Numerical modelling

A 3D FEM of the bridge is developed in Abaqus [43] by considering both geometrical and mechanical nonlinearities. Solid C3D8R elements (8-node linear, reduced integration, hourglass control) are used to model the bridge components. The mesh dimensions are kept in the range between 0.35 m and 0.75 m as per previous studies by Milani and Lourenço [13] and Scozzese et al. [26] in order to provide a good balance between the computational burden and the accuracy.

A macro-modelling approach is used for the masonry components (foundations, pier, arch barrel, spandrel walls, abutments), with the nonlinear mechanical behaviour described by the concrete damaged plasticity (CDP) model [44,45] available in Abaqus manual [46]. The masonry is considered as a homogenous material with no distinction between units and mortar. Thus, the parameters of the masonry components highlighted in Table 1 describe the behaviour of the composite masonry material.

The CDP model is a coupled plasticity-damage model that is widely employed for describing the behaviour of brittle materials that can fail due to compressive crushing and tensile cracking, such as concrete and masonry. Fig. 4 illustrates the uniaxial stress-strain responses of the masonry components in compression and tension. Both the responses are characterised by an initial linear elastic behaviour, controlled by the Young Modulus (E). Under uniaxial compression, the "yield" stress σ_{c0} denotes the end of the linear elastic behaviour, and σ_{cu} denotes the peak response, which is followed by a nonlinear softening response as in Fig. 4a. The damage parameter d_{c0} controls the unloading and reloading stiffness under uniaxial compression. It should be noted that the damage is not activated in the analyses, causing the masonry material to exhibit fully plastic behaviour under compression. Under uniaxial tension, σ_{t0} denotes the cracking stress. The damage parameter d_{t0} controls the unloading and reloading stiffness under uniaxial tension (see Fig. 4b). Although various laws could be used for describing the softening, in the analyses a linear softening behaviour, controlled by the fracture energy g_f, is considered. Further details about the CDP model can be found in the Abaqus manual [46].

The material properties assigned to the masonry bridge components (arches, piers, and spandrels abutment and the backfill) are based on typical values from the literature [11–13,26]. Fig. 5 shows the meshed model and the cohesive elements at the base of the pier foundation. The following mechanical parameters are reported in Table 1: density (ρ), Young's modulus (E), "yield" compressive strength (σ_{c0}), peak compressive strength (σ_{cu}), peak tensile strength (σ_{t0}) of masonry and backfill, tensile fracture energies (g_f) of masonry, friction coefficient (μ), normal stiffness per unit area (k_n), tangential and shear stiffnesses (k_t, k_s) of the backfill-masonry contact interfaces. A sensitivity study is also carried out to estimate the effect of variations of these parameters on results.

A realistic representation of the behaviour of the backfill and its interaction with the arch barrel and the spandrel walls is essential for an accurate prediction of the response of masonry arch bridges (see, e.g., [47,48]). The elastic response is described using Young's modulus of 250 MPa and Poisson's ratio of 0.2, while the plastic behaviour is modelled using a Mohr-Coulomb yield criterion. A linear elastic model with a Mohr-Coulomb failure criterion (friction angle ϕ=60° and cohesion c_b =10 kPa) is employed for the backfill material.

Nonlinear frictional/cohesive interfaces [11,22] are used to simulate the interactions between adjacent components of the bridge (arch--to-pier, spandrel-to-pier, spandrel-to-arch, and masonry-mortar interfaces) as shown in Table 1. These zero-thickness interfaces are a lumped representation of the mortar joints located between the above-mentioned bridge components.

A simplified Winkler subgrade modelling approach is employed to describe the soil-structure interaction and the effects of scour, using cohesive elements with linear elastic behaviour (uncoupled responses along the different directions) and zero tensile resistance at the base of the foundation, similarly to [11]. Infinite resistance is assigned in the shear direction. The cohesive elements are introduced at the foundations of both the piers and abutments to avoid non-uniform settlements. The proposed modelling strategy has been employed in many past studies [11,12,24–26] and has been validated with experimental results [49] and comparisons with more advanced strategies [50]. Reference can be made to Tubaldi et al. [11] for a comparison between alternative strategies for modelling the soil-structure interaction problem in presence of scour.

As per FEMA 356 guidelines [51], the subgrade stiffness parameters are estimated by the analytical formulation of Gazetas [52]. The vertical (axial) subgrade reaction is calculated as $k'_{s_v} = \frac{k_{s_v}}{LB} = 0.15$ N/mm^3, where k_{s_v} denotes the vertical translational impedance of a rigid foundation with length L, width B, and $L > B$ [11]. Similarly, the two horizontal subgrade reactions $k'_{s_{hz}}$ and $k'_{s_{hx}}$ in shear directions are evaluated to be 0.86 N/mm^3 and 0.24 N/mm^3, respectively. It is noteworthy that a relatively stiff soil has been considered in the calculations.

4. Traffic load analysis

4.1. Load modelling

Traffic loading is a key variable in structural design and assessment of roadway bridges. European standards provide load model 1 (LM1) as a conventional TLM for global safety checks of bridges [53]. The first notional lane of LM1, with 3-m width, is defined by a tandem axial load of 600 kN (i.e., 300 kN + 300 kN) combined with a uniformly distributed load (UDL) of 9 kN/m^2. LM1 does not aim at representing actual vehicles, since it is calibrated based on simulations of effects of traffic streams, having as target a return period of 1000 years, corresponding to a 5 % probability of occurrence in 50 years [53].

Apart from LM1, three additional TLMs are considered in this study

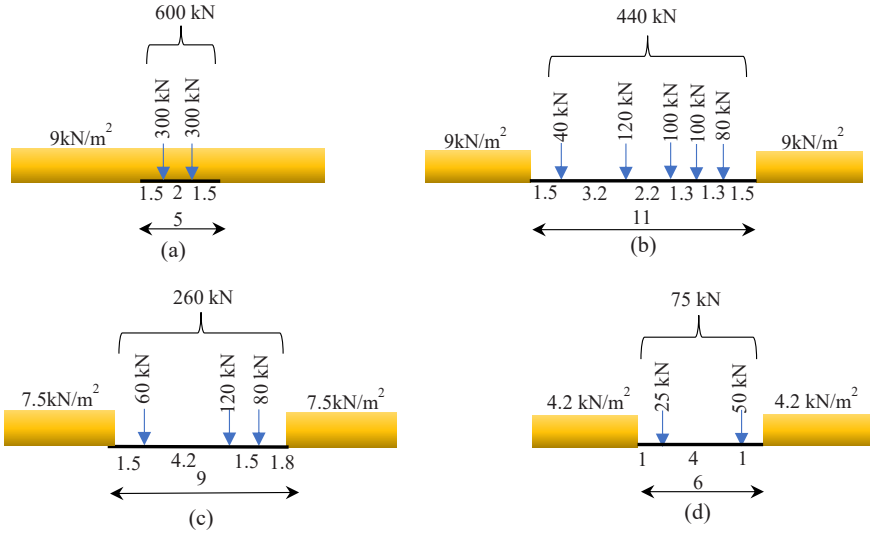

Fig. 6. Adopted traffic load models (distance in m): (a) LM1 (b) heavy (5-axles) TLM, (b) medium (3-axles) TLM, (d) light (2-axles) TLM.

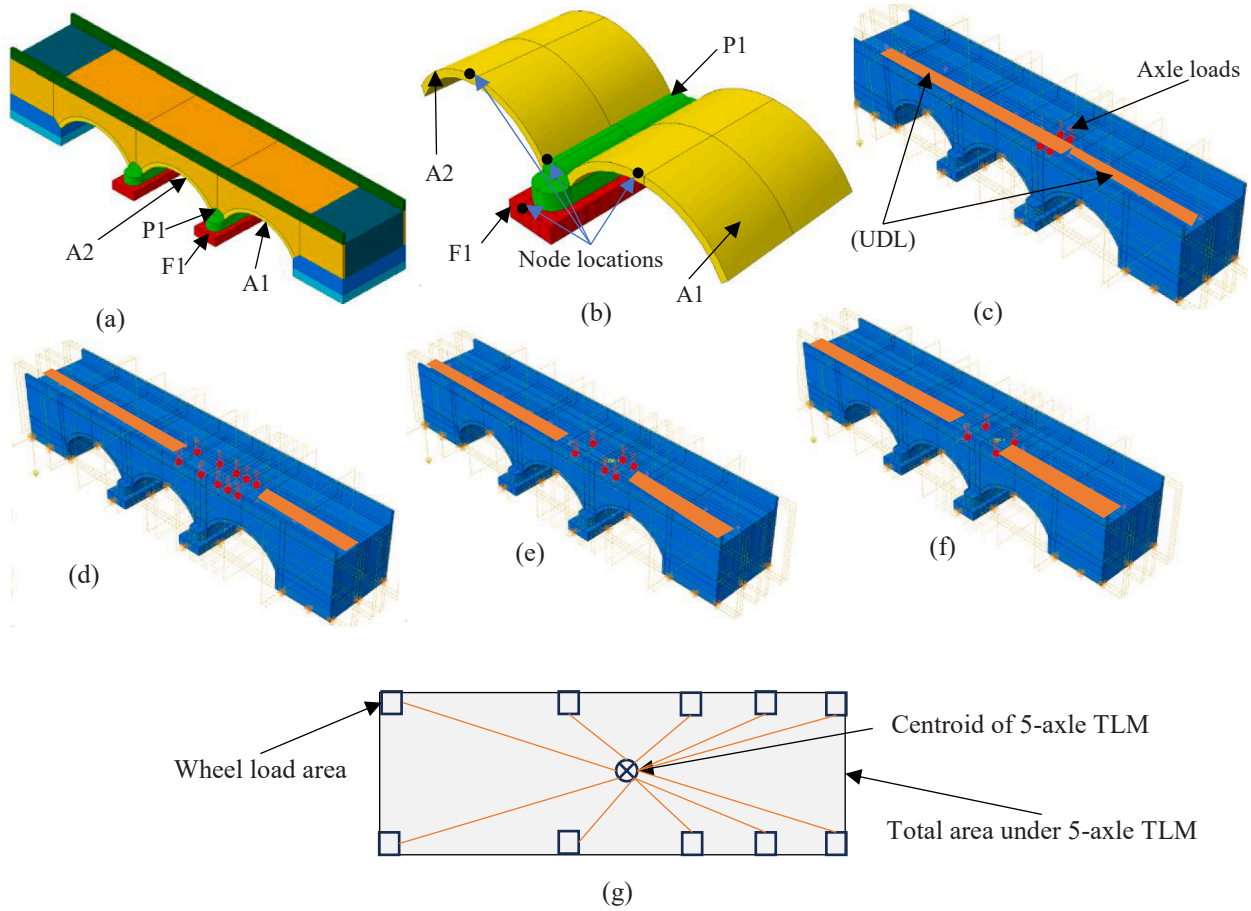

Fig. 7. Numerical model: (a, b) control sections and node points for displacement monitoring; (c) LM1; (d) 5-axles TLM; (e) 3-axles TLM; (f) 2-axles TLM; and (g) rigid body constraints showing tie surfaces (wheel areas) and the reference node (centroid of the point loads).

that are representative of common actual vehicles from the Italian stock [6,8], namely a heavy vehicle (5 axles with gross vehicle weight (GVW) equal to 440 kN), a medium vehicle (3 axles with GVW = 260 kN), and a light vehicle (2 axles with GVW = 75 kN), respectively (Fig. 6). In addition to point loads modelling the load transferred by the wheels of a single vehicle of each class, a UDL is applied at the sides of the silhouette to represent an equivalent distributed load for the same vehicle class [8]. Since such TLMs would represent traffic congestion, no dynamic load allowance is considered unless a single vehicle (i.e. only point loads with no UDL) would provide more adverse conditions in which case an amplification factor up to 1.4 has to be adopted [7].

In all TLMs, the point loads are imposed as pressure loads, each acting on a square area having 400 mm base length representative of the wheel-pavement contact area. Four control sections (see Fig. 7a) are

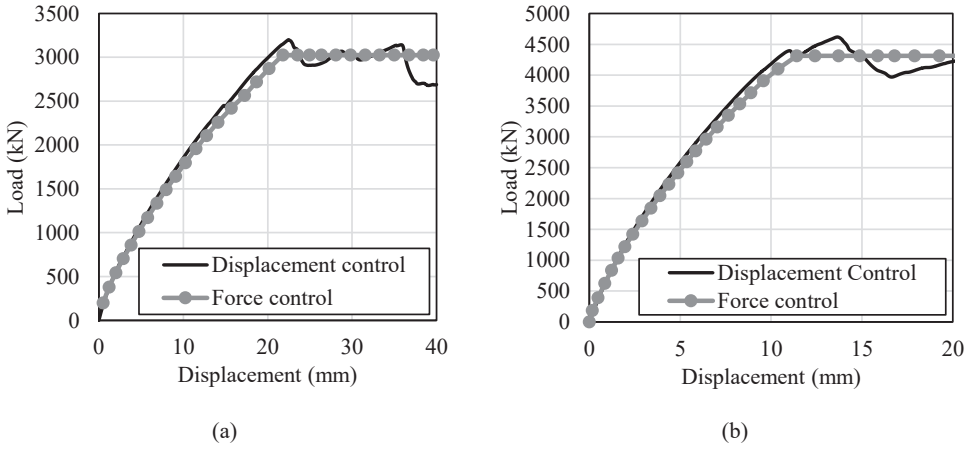

Fig. 8. Load–displacement curves corresponding to force and displacement control strategies under different traffic load models: (a) LM1; (b) 5-axles TLM.

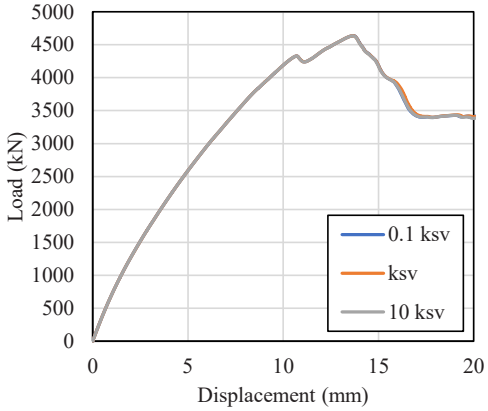

Fig. 9. Comparison between load–displacement curves corresponding to different values of vertical subgrade stiffness k_{sv}.

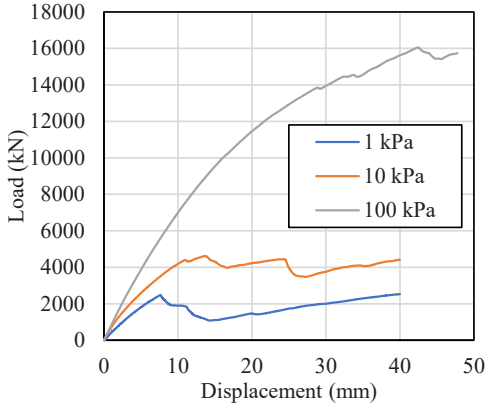

Fig. 10. Comparison between load–displacement curves corresponding to different values of backfill cohesion c_b.

selected to monitor displacements and internal stresses in the bridge components: P1 (pier top), A_1 and A_2 (arch crowns of the arches connected to P1), and F1 (foundation below P1). Fig. 7(b-e) show the TLMs considered acting on a single 3-m-wide lane on the upstream side of the bridge model (the second notional lane is not loaded), providing the worst conditions in combination with scour acting on the same side.

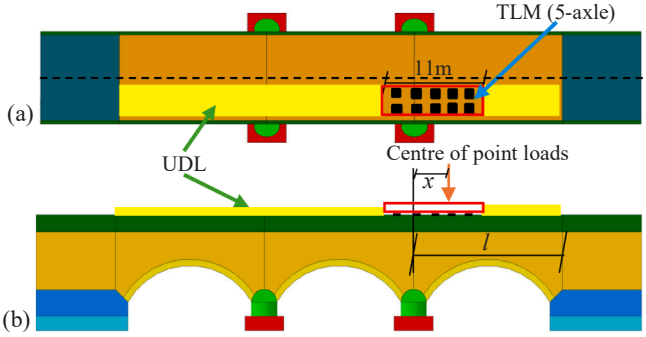

Fig. 11. (a) Top view and (b) side view of the bridge showing the position of the 5-axles TLM.

4.2. *Parametric study under traffic load*

Several parameters can affect the estimated capacity of the bridge including – among the others – the analysis' control strategy, the subgrade stiffness of the foundation, the backfill cohesion, and the position of the TLM along the bridge. The following parametric study investigates the influence of the above-mentioned parameters.

4.2.1. *Influence of analysis control strategy*

To determine the capacity of the masonry bridge under traffic load only, LM1 and 5-axles TLM are applied to the model with the resultant of the point loads acting above P1. Both displacement-controlled and force-controlled methods are adopted to estimate the bridge capacity assumed as the sum of the vertical support reactions (also equal to total imposed load in a force-controlled analysis) due to increasing traffic loading. Under displacement control strategy, the UDL is kept constant along the full length of the backfill (Fig. 7c-f), whereas the downward displacement of the control joint located at the centroid of the constrained wheel areas (see Fig. 7g) is progressively increased up to bridge collapse. Under force-controlled method, a pressure load is applied on the wheel area in terms of time-load history, and the peak capacity of the bridge is estimated by keeping the UDL constant. Fig. 8 shows the comparison of capacity curves estimated using the two methods. A very good agreement is observed up to peak load. Force control slightly underestimates the load capacity compared to displacement control by 5.8 % and 7.1 % for LM1 and 5-axles TLM, respectively. The subsequent analyses are carried out under displacement control, in order to evaluate the behaviour beyond the first peak.

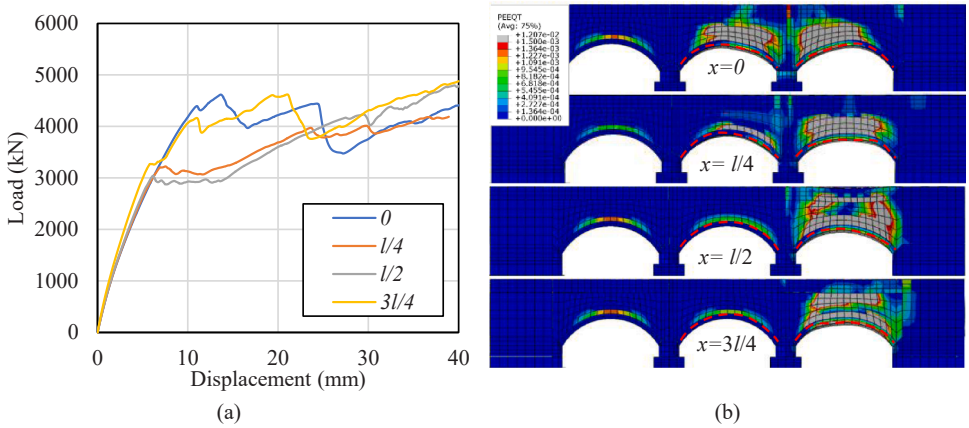

Fig. 12. Comparison of (a) load–displacement curves and (b) PEEQT distribution showing arch deformation profile (red dashed line) under varying position of the 5-axle TLM recorded at a displacement of 40 mm.

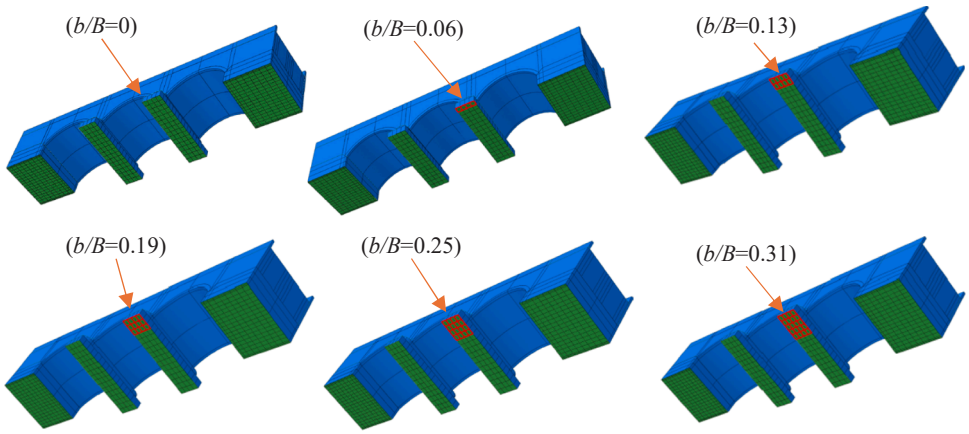

Fig. 13. Abutment and foundation boundary conditions and progressive removal of supports at F1 representing settlements ($0 < b/B < 0.31$).

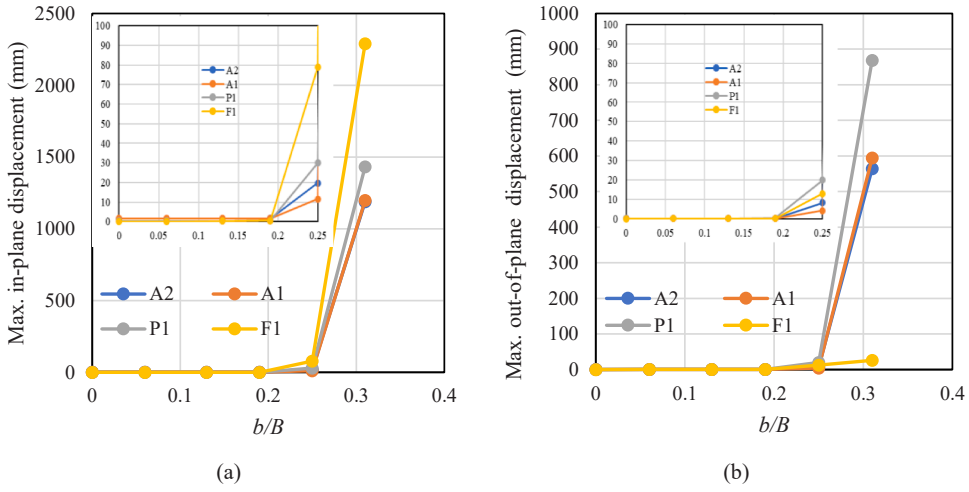

Fig. 14. (a) In-plane and (b) out-of-plane displacement recorded at the selected control sections of the bridge.

4.2.2. Sensitivity to vertical subgrade stiffness

In order to evaluate the influence of subgrade stiffness parameter on the bridge capacity under traffic loading, three models are developed with cohesive elements under the foundation assigned a value of the subgrade reaction of $0.1k_{sv}$, k_{sv} and $10\,k_{sv}$. Since there is no significant difference in terms of capacity curves obtained for the 5-axles TLM (see Fig. 9), it can be stated that the global bridge performance is not significantly affected by soil-structure interaction model parameters. It is noteworthy that the obtained result is not in line with the findings of other studies, showing the significant influence of the role played by the soil on the bridge behaviour (see e.g. [16]). Nonetheless, the outcome of this study depends on the assumption of a relatively stiff soil.

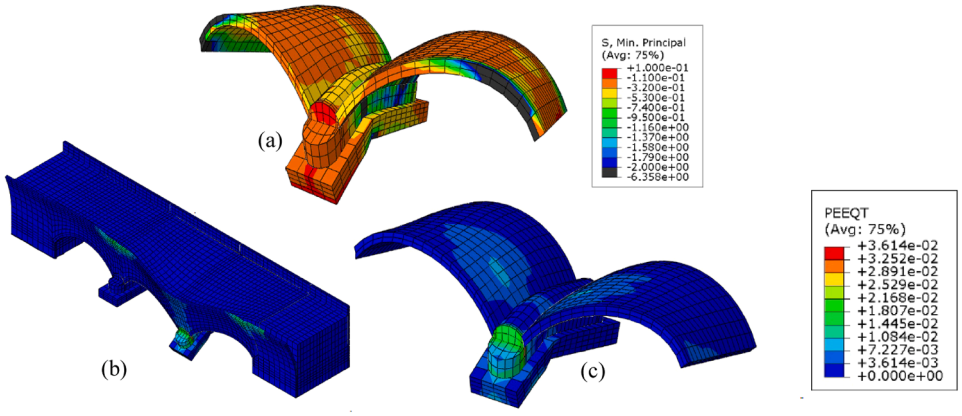

Fig. 15. (a) Peak compressive stress distribution (MPa), and (b, c) PEEQT distribution for $b/B = 0.31$.

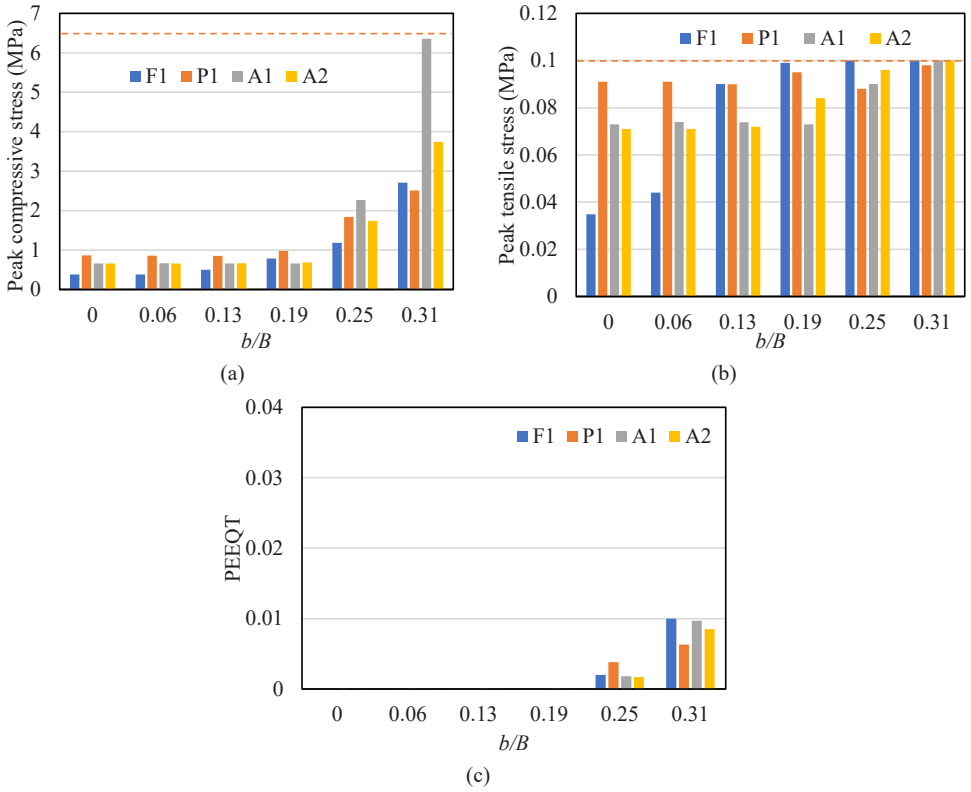

Fig. 16. (a) peak compressive stress (b) peak tensile stress (c) PEEQT for selected sections of the bridge under increasing b/B.

4.2.3. Sensitivity to backfill cohesion

In this section, the influence of the cohesion of the backfill material is studied by changing its value (10 kPa) by a factor of 10 and 1/10. Three different models are analysed with cohesion equal to 1 kPa, 10 kPa and 100 kPa, respectively. It can be seen from Fig. 10 that the capacity of the bridge is significantly affected by the cohesion value: when the c_b reduces from 10 kPa to 1 kPa, the capacity of the bridge reduces by half. An increase in c_b from 10 kPa to 100 kPa increases the capacity by 3.5 times. It is noteworthy that a very low backfill cohesion leads to significant increase of computational time and convergence issues. For this reason, the value $c_b = 10$ kPa (Table 1) is adopted for the model, providing a good balance between computational time and accuracy. Adopting lower values of c_b does not result in significant changes in the capacity curve. The high sensitivity of the bridge capacity to the backfill cohesion (Fig. 10) has been observed in other studies on the same issue [11,25].

4.2.4. Sensitivity to TLM position along the bridge

A simplified influence line study is conducted to assess the effects of traffic load moving along the span length (l) of the bridge. Four models are developed for the 5-axles TLM. In the reference case, the TLM is applied with the resultant of point loads acting on top of P1 (i.e., $x = 0$). In the other three models, the TLM is applied with its resultant at a distance $x = l/4$, $x = l/2$, and $x = 3\,l/4$ from P1 along a horizontal plane. Fig. 11 illustrates top and side views of the bridge with TLM position.

Fig. 12a shows the estimated load–displacement capacity curves for the selected traffic load positions, with the displacement measured at the centre of the TLM. The highest load capacity (equal to 4618 kN) is obtained for the TLM positioned on top of P1. When the centroid of the TLM moves towards the crown and reaches $x = l/4$, the capacity is reduced by 30 %. At $x = l/2$, the least value of capacity (3042 kN) is observed, which is 35 % lower than the case $x = 0$. For $x = 3\,l/4$, the

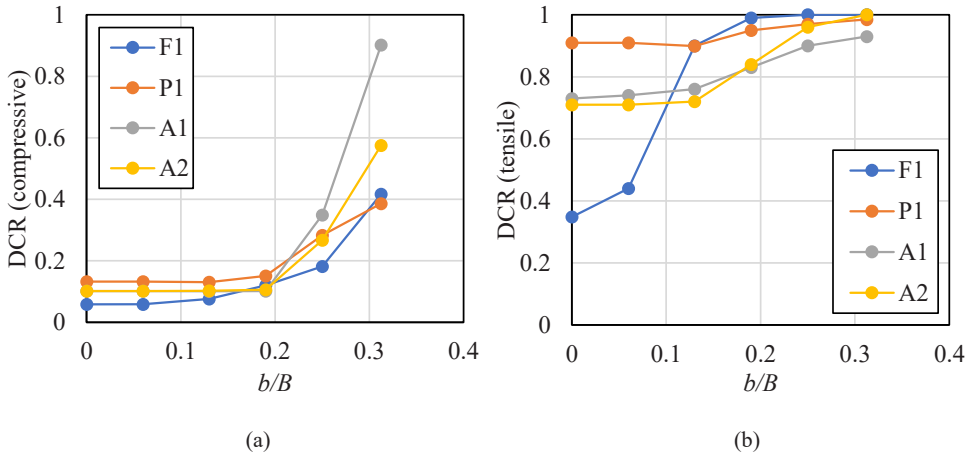

Fig. 17. (a) compressive DCR and (b) tensile DCR under increasing *b/B*.

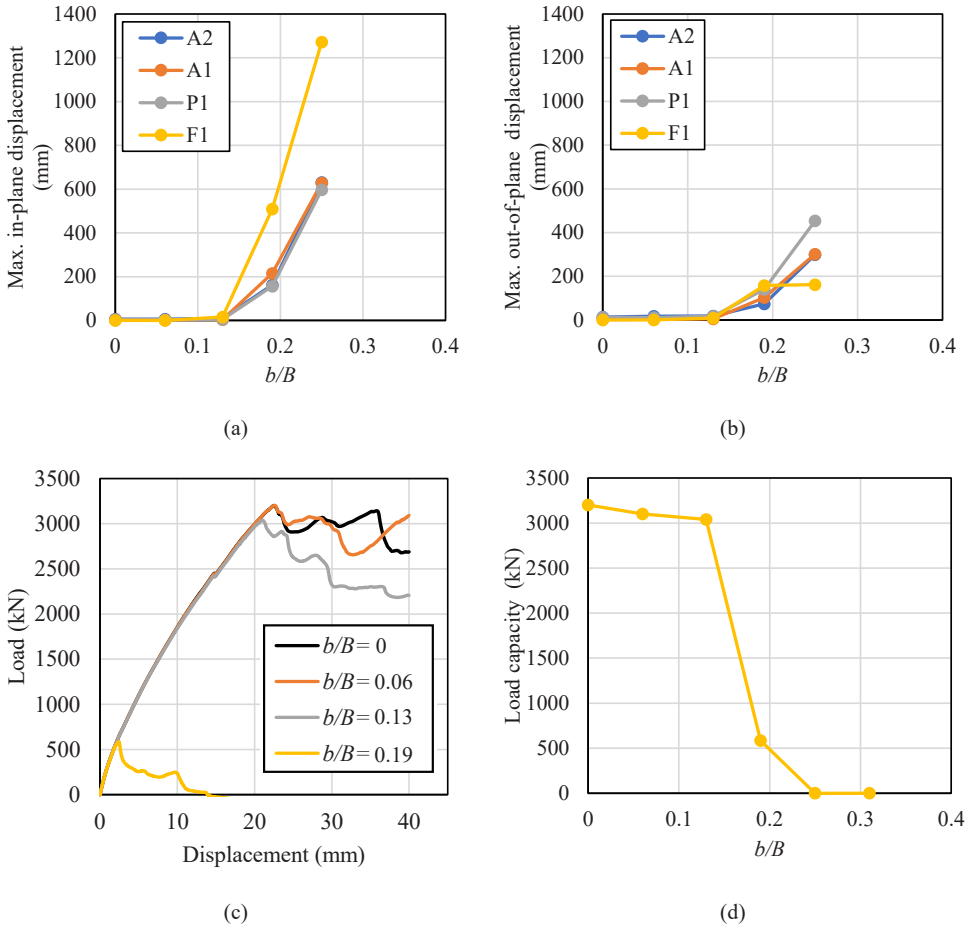

Fig. 18. (a) In-plane and (b) out-of-plane displacement recorded at selected sections of the bridge, (c) load-displacement curves and (d) load capacity of the bridge under increasing *b/B*.

peak load capacity is found to be increased and approaches to the case $x = 0$ while resulting in slightly higher stiffness. Subsequent analyses discussed in the following sections of this paper are carried out by assuming the centroid of the TLM to be located at $x = 0$ to provide maximum effects on the scoured pier P1. In fact, for significant scour levels, the condition $x = 0$ is the one resulting in the lowest bearing capacity among the various possible positions of the TLM, as demonstrated by the sensitivity analysis reported in Section 6.4.

Fig. 12b shows the equivalent plastic strain distribution (PEEQT) in the arch barrel, highlighting the arch deformation profile for the selected positions of the TLM. At $x = 0$, the plastic strains are symmetrically distributed over the arches (A1 and A2) and the spandrel walls with higher concentrations at the P1. When the TLM centroid moves to $x = l/4$, the critical section is close to A1 and attached spandrel wall. The case $x = l/2$ yields the highest level of plastic strains associated with the minimum load bearing capacity.

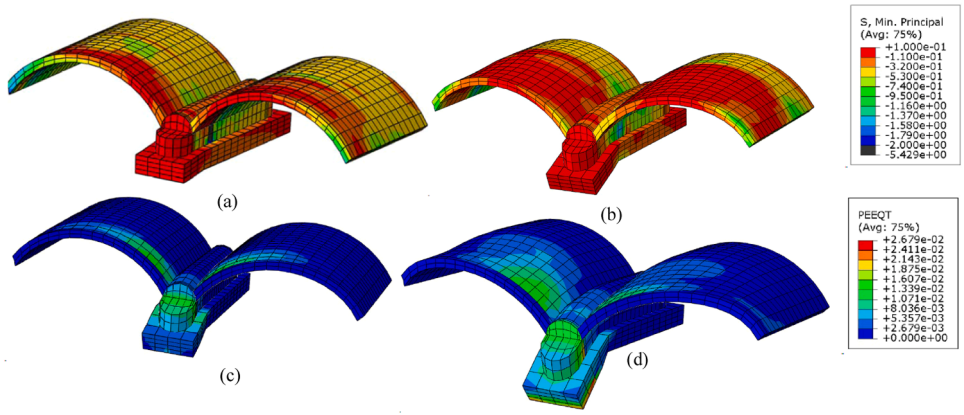

Fig. 19. (a, b) Peak compressive stress (MPa) and (c, d) PEEQT distribution for $b/B = 0.19$ and $b/B = 0.25$.

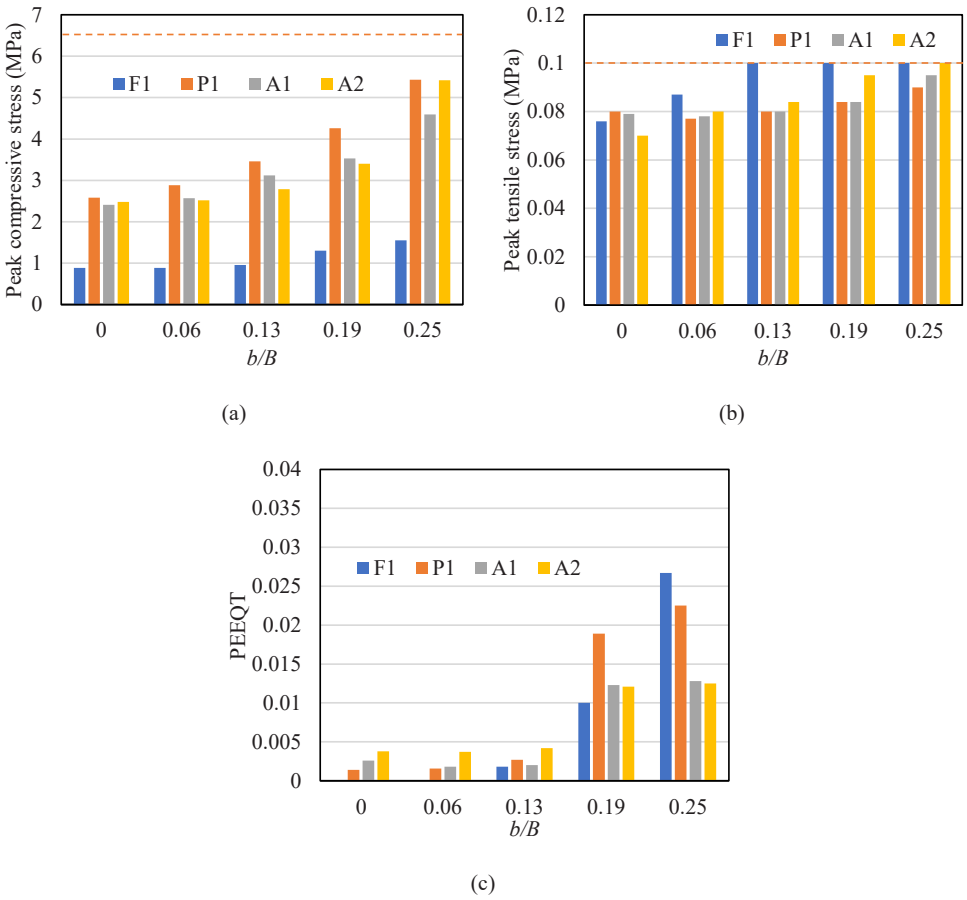

Fig. 20. (a) Peak compressive stress, (b) peak tensile stress and (c) PEEQT at selected sections of the bridge under increasing b/B.

5. Scour analysis

Scour is assumed to occur at the foundation of pier P1. In the initial stage, only the gravity loads are applied (step 1). Then, the scour action is simulated by removing the cohesive elements that describe the interaction between the foundation base and the surrounding soil. The dimensionless parameter b/B, representing the ratio between the scoured foundation length b over the total foundation length B along the direction of the flow, is used to describe the evolution of scour. Increasing discrete levels of b/B are considered, in the range between 0 (value corresponding to the case of no scour) and 0.31 (value resulting in very large displacements and plastic deformations in the model under permanent loading and assumed to represent bridge collapse), as illustrated in Fig. 13.

The maximum in-plane and out-of-plane displacements are recorded for the selected sections of the bridge (P1, A1, A2 and F1) for increasing values of b/B (see Fig. 14). No significant displacements are observed for b/B lower than 0.19, whereas for larger values all these parameters increase significantly for increasing scour levels. The largest in-plane vertical displacements are observed at F1 followed by P1, A1 and A2 with peak values corresponding to $b/B = 0.31$. Similarly, the largest out-of-plane horizontal displacements are observed at P1 followed by A2, A1 and F1. Once b/B reaches 31 %, many response parameters significantly increase and numerical converge issues arise, so this condition is

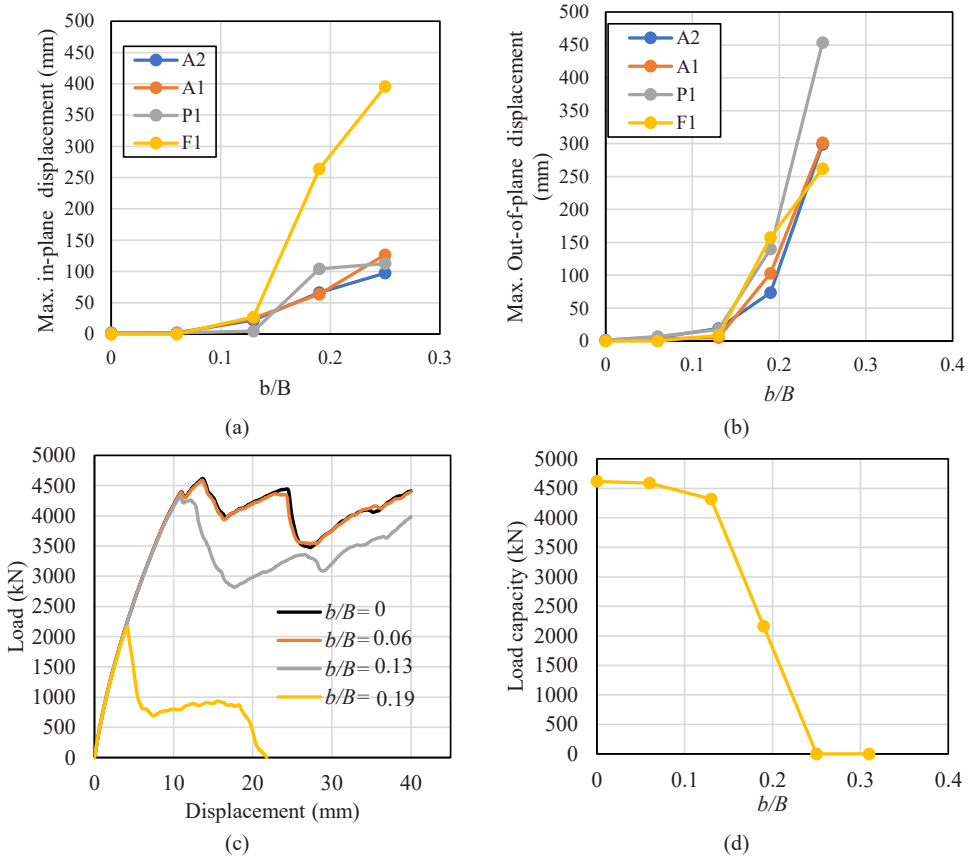

Fig. 21. (a) In-plane and (b) out-of-plane displacements recorded at selected sections of the bridge, (c) load–displacement curves and (d) load capacity of the bridge under increasing *b/B*.

assumed representative of the bridge collapse due to scour.

In terms of peak compressive stress distribution, there is no visible stress concentration up to $b/B = 0.19$, and the stress contours are symmetrically distributed across the bridge. Once *b/B* reaches 0.19, high non-uniform concentration of stresses arises in P1, F1, A1 and A2, until the critical condition is attained for $b/B = 0.31$ (Fig. 15a). In terms of tensile equivalent plastic strains (PEEQTs), the condition $b/B = 0.25$ results in visible strain concentrations at the foundation (F1), pier (P1) and spandrel wall. The contour plots of PEEQTs at $b/B = 0.31$ are shown in Fig. 15b,c. The failure mechanism involves the pier P1 above the scoured length and the two adjacent arches.

In order to analyse the local behaviour of the bridge components, the values of the peak compressive stress, peak tensile stress and equivalent plastic strain recorded at F1, P1, A1 and A2 are compared to each other under increasing values of *b/B* (Fig. 16). In general, the compressive and tensile stresses do not increase much for increasing values of *b/B* when *b/B* is less than 0.19. For values increasing beyond 0.19, a significant increase in stresses is observed. Tensile cracks start to appear for values of *b/B* slightly higher than 0.19.

Fig. 16a shows the variation of compressive stresses. For $b/B = 0.31$, the maximum compressive stresses, localised in correspondence of A1, are about 6.35 MPa, which is slightly lower than the assumed compressive strength for masonry. The abutments and the arches experience the highest increase of stresses due to scour. Fig. 16b shows the peak tensile stresses at the various locations and scour levels. The first cracks appear in the foundation (F1), but for $b/B = 0.31$, cracking is observed also in the piers (P1) and arches (A1 and A2). It can be seen from Fig. 16c that no plastic strain is obtained up to $b/B = 0.19$ accordingly. However, beyond $b/B = 0.25$, PEEQT starts increasing significantly and reaches the value of 0.01 at $b/B = 0.31$.

Fig. 17(a) shows the compressive demand-to-capacity ratios (DCRs) for all the selected sections of the bridge under increasing *b/B*. DCR is herein assumed to be the ratio between the peak compressive (tensile) stress and compressive (tensile) strength of masonry. The increase in DCR for compression appears to be rather small up to $b/B = 0.19$ but, once *b/B* goes beyond 0.25, the trend becomes exponential due to higher nonlinearity effects. Similar observations can be seen from Fig. 17(b), showing the tensile DCR under varying *b/B*.

6. Robustness assessment based on residual traffic load capacity under scour

In order to study the structural robustness and hence residual traffic load capacity of the scoured bridge, incremental TLMs are applied on the bridge deck (above P1) after imposing each scour level, corresponding to discrete values of *b/B* ranging from 0 to 0.31.

6.1. LM1 on scoured bridge

Fig. 18a and b show a comparison of the in-plane and out-of-plane displacements recorded at P1, A1, A2 and F1 with the bridge already subjected to scour when loaded by LM1 in displacement-controlled mode. Fig. 18c and d show that for levels of *b/B* up to 0.13, the peak capacity remains almost unchanged, whereas for $b/B = 0.19$ a 80 % drop in capacity is found compared to the unscoured case. For $b/B = 0.25$, the bridge cannot withstand any traffic loading after imposing scour effects. It is noteworthy that the collapse condition due to scour only (and gravity loads) is identified in correspondence of higher *b/B* levels, of the order of 0.31. Thus, for $b/B > 0.25$, although the bridge may not collapse under its own weight, it would collapse at the passage of traffic.

Fig. 19 a-b shows the peak compressive stress distribution of the model under LM1 subjected to scour. Once *b/B* reaches 0.19, high non-

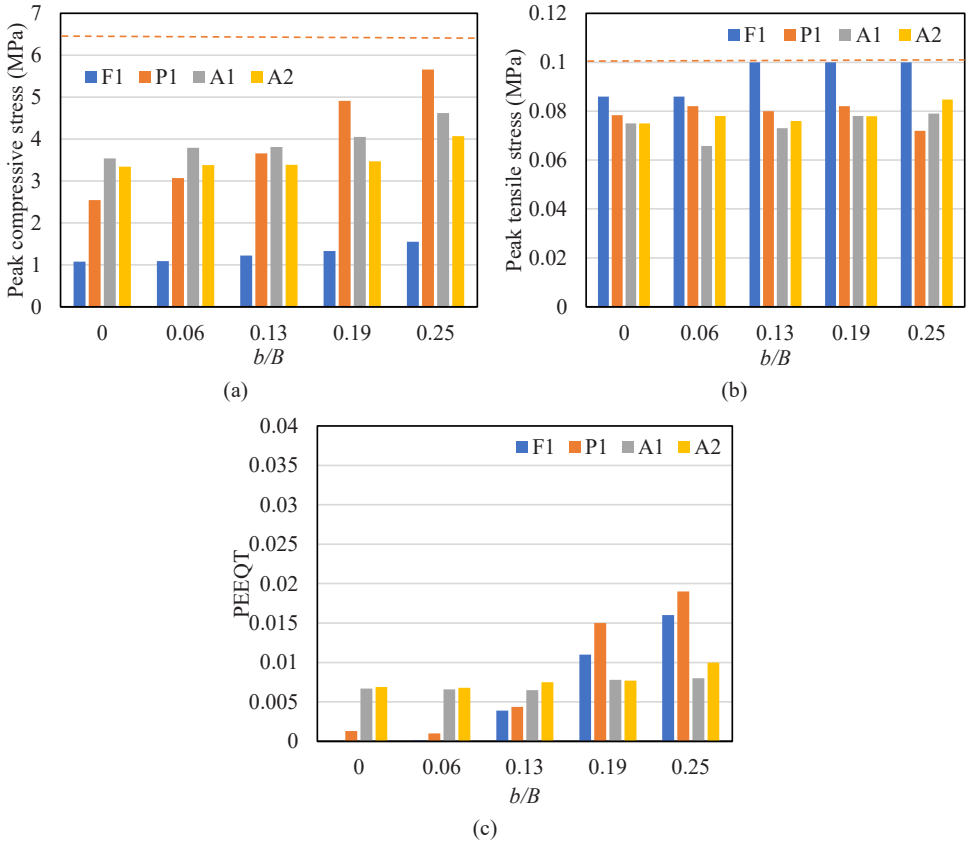

Fig. 22. (a) Peak compressive stress, (b) peak tensile stress, (c) PEEQT at selected sections of the bridge under increasing b/B.

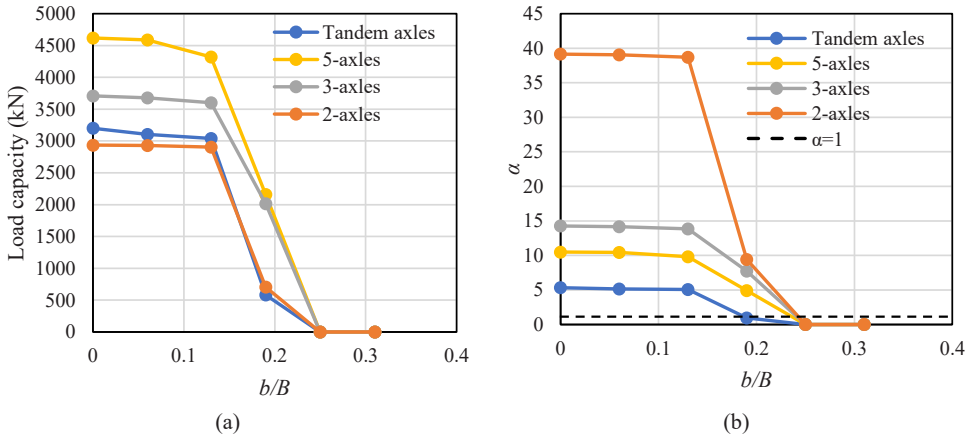

Fig. 23. Interaction domains corresponding to different TLMs under increasing scour levels in terms of (a) peak load capacity and (b) traffic load factor.

uniform concentrations stresses are visible and at b/B= 0.25 a failure mechanism is observed. Similarly, no visible plastic strains are observed up to $b/B = 0.13$. However, beyond $b/B > 0.19$, plastic strains are seen at the foundation (F1), pier (P1), arches (A1 and A2) and spandrel walls.

Fig. 18d shows that once b/B reaches 0.25, the traffic load capacity reaches zero; therefore, response parameters for the selected sections of bridge are presented up to such a level of scour in Fig. 20. In particular, Fig. 20a-b show an increasing trend of peak compressive stress and peak tensile stress under increasing b/B in the selected sections. Fig. 20c shows the equivalent plastic strain distribution with very low values up to $b/B = 0.13$: beyond this value, damage starts increasing significantly and a peak plastic strain value of 0.027 is recorded for $b/B = 0.25$. This value is one order of magnitude larger than that due to scour only.

6.2. *5-axles TLM on scoured bridge*

The 5-axles TLM provides a useful representation of heavy commercial vehicles with GVW = 440 kN as per Italian road code limitations. Fig. 21a and b show a comparison of in-plane and out-of-pane displacements recorded at A1, A2, P1 and F1 subjected to scour under 5-axles TLM. A similar trend in both displacements and load-bearing capacity is found compared to LM1, i.e., no capacity reduction up to 13 % loss of foundation length. The capacity exhibits a 50 % drop at b/B = 0.19 and reduces to zero under $b/B = 0.25$ (Fig. 21 c-d). The same trend as previously observed under LM1 is obtained in terms of peak stresses and equivalent plastic strain distribution (see Fig. 22). For the sake of brevity, results under 3-axles and 2-axles TLMs are reported in

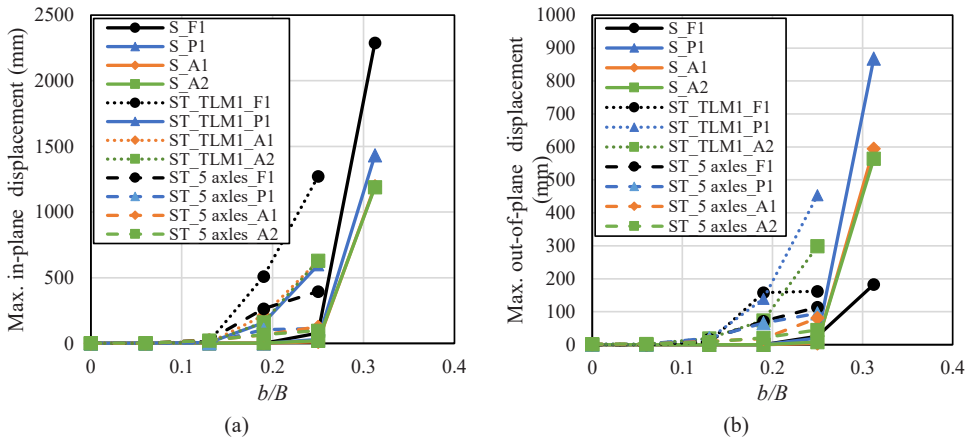

Fig. 24. (a) In-plane and (b) out-of-plane displacements recorded for selected sections of bridge with increasing b/B and different TLMs.

the following section in terms of load-bearing capacity compared to LM1 and 5-axles TLM.

6.3. Influence of different TLMs on global response

Fig. 23a shows the peak load capacity against traffic load under different levels of scour depth, representing an interaction domain between the scour level (x-axis) and the TLM-related load-bearing capacity (y-axis). It can be noted that for a given b/B, the point loads position of the given TLM plays a major role on load capacity under incremental static analysis in displacement control. For this reason, 2-axles TLM and LM1 yields very similar results and the lowest capacity curves since both present two axles at a small distance in the longitudinal section.

From a structural safety standpoint, a normalized TLM capacity parameter can be defined in terms of traffic load factor (or multiplier) α, consistently with Miluccio et al. [54]. This is the multiplier of the axle loads of each TLM that corresponds to the peak in the force-displacement curve (while assuming constant UDL). Hence, α can be interpreted as a robustness measure, such that the structure is deemed robust to scour if $\alpha \geq 1$, highlighting its ability to withstand design traffic loads under scour-induced damage. For every scour level, the lowest value of α is obtained for LM1 (see Fig. 23b), followed by the 5-axles, 3-axles, and 2-axles TLM, confirming an expected trend due to the decreasing magnitude of the different TLMs. These results may be of use to bridge operators for defining scour thresholds triggering traffic restrictions and bridge closure. Up to $b/B = 0.13$, no restriction would be required because the overall capacity is slightly affected by scour and the bridge safety is ensured under all TLMs, meaning that code-conforming safety levels for new design would be obtained (i.e., $\alpha \geq 5$). As b/B increases from 0.13 to 0.19, α significantly reduces and drops to almost 1 under LM1, resulting in safety levels lower than those prescribed for new design. In this case, any restrictions to actual vehicular classes can avoid the bridge closure by proper limitations to GVW.

For 5-axles, 3-axles, and 2-axles TLMs, the condition $b/B = 0.19$ yields a value of $\alpha \geq 5$, demonstrating adequate safety levels against collapse even in case a dynamic load allowance is considered. For $b/B = 0.25$, the residual capacity drops to zero regardless of the selected TLM because scour effects become dominant. This outcome would suggest traffic limitations to very heavy vehicles (e.g., GVW < 440 kN) in case of scour depths in the range between 0.13 and 0.19, and no restrictions required for $b/B < 0.13$.

In terms of collapse mechanism, in-plane and out-of-plane displacements at F1, P1 A1 and A2 under increasing value of b/B are compared considering the cases of scour only (S), scour combined with LM1 (ST_TLM1), and scour combined with 5-axles TLM (ST_5 axles). In the range $0.13 < b/B < 0.25$, the highest rate of increase of in-plane displacements recorded at the selected sections is observed under scour combined with LM1, followed by scour combined with 5-axles TLM (Fig. 24a). Significant influence of the TLMs on scour is observed causing early failures compared to scour only condition. This comparison confirms that the case $b/B = 0.25$ would not be critical when only scour is acting combined with self-weight up to $b/B = 0.31$.

In case of a scour level $b/B = 0.25$, any traffic load passing on the bridge can trigger a global collapse mechanism. A similar trend can be seen for the out-of-plane displacements (see Fig. 24b).

6.4. Sensitivity analysis

A parametric study is conducted to estimate the capacity of the bridge under scour combined with the 5-axles TLM for varying masonry tensile strength values (σ_t), masonry fracture energy in tension (g_f), backfill cohesion (c_b) and position of traffic loading along the length of the bridge (see Fig. 25). It can be seen from Fig. 25a that the model is sensitive to the selected magnitude of the masonry tensile strength. A 10 % decrease in the peak load capacity of the bridge is observed when the tensile strength is reduced to half, i.e., from 0.1 MPa to 0.05 MPa. When tensile strength is doubled, an increase of 12 % in load capacity is observed. Again, as b/B increases, the load capacity drops down and the rate of decrease in the capacity is the highest for $\sigma_t = 0.05$ MPa caused by early tensile failure in the masonry as compared to other cases. However, when tensile strength is $\sigma_t = 0.2$ MPa, the bridge can take 20 % of its peak capacity even under $b/B = 0.25$.

Fig. 25b demonstrates the influence of the masonry fracture energy considered in the model. To study this, five different levels of fracture energies are considered and analysed. Higher fracture energy leads to higher capacity prediction. Up to a fracture energy of 0.01 N/mm, the bridge is unable to take any further traffic load under $b/B = 0.25$. However, if $g_f > 0.025$ MPa·mm, the bridge still keeps one-third of its peak load capacity.

Fig. 25c shows the comparison of predicted bridge capacity subjected to scour at three levels of backfill cohesion (i.e., 1 kPa, 10 kPa, and 100 kPa). It can be seen that backfill cohesion has significant influence on the capacity of the bridge because the peak capacity drops by 46 % when c_b reduces by 10 times, i.e., from 10 kPa to 1 kPa. Again, the lowest value of c_b (i.e., 1 kPa) caused early failure for which the load capacity goes to zero even under $b/B = 0.13$. However, if c_b is increased by 10 times (i.e., reaching 100 kPa), a 250 % increase in load capacity is observed with 23 % residual capacity even under $b/B = 0.25$.

Fig. 25d demonstrates the influence of traffic load position on the performance of the scoured bridge. Referring to the Section 4.1.4, the highest level of capacity (4618 kN) is observed when the centroid of the TLM is at $x = 0$, followed by $x = 3\,l/4$, $x = l/4$ and $x = l/2$, respectively. The load capacity is evaluated under increasing b/B levels by

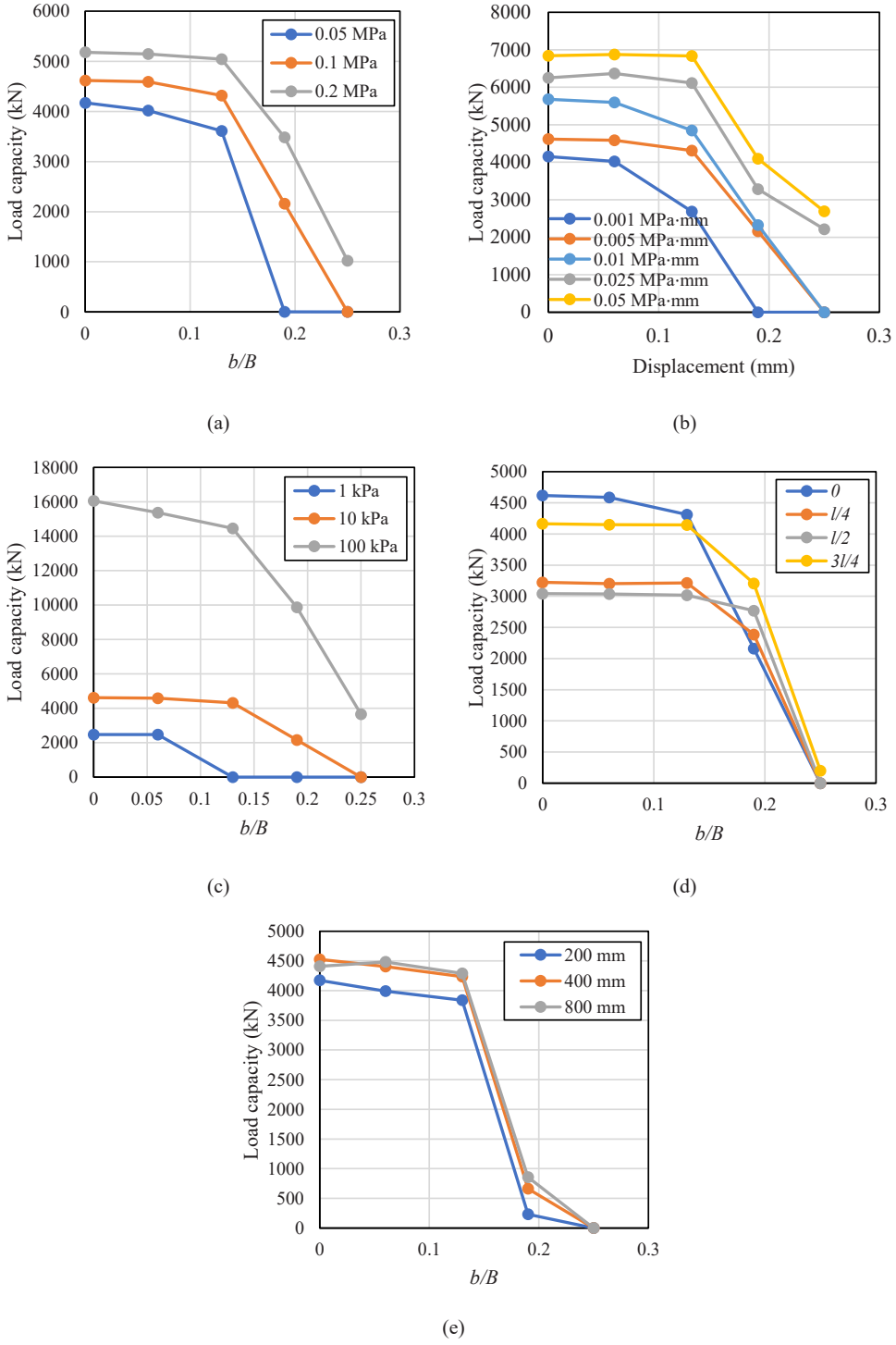

Fig. 25. Influence of (a) masonry tensile strength, (b) fracture energy, (c) backfill cohesion, (d) position of traffic loading, and (e) mesh size under increasing b/B.

considering the TLMs at the four selected locations discussed above. The case corresponding to $x = 0$ corresponds to the highest level of capacity for zero scour, but also to the highest level of decrease in capacity as the scour is considered just below the pier P1, where the centroid of TLM is located. This leads to the condition where the TLM with $x = 0$ produces the lowest load carrying capacity under $b/B = 0.19$.

Fig. 25e shows the influence of mesh size selection on the capacity prediction of the bridge. Parts with complex shapes are cut into simpler, more regular shapes to facilitate the automatic meshing process. Sensitivity analysis considering a mesh size range between 200 and 800 mm demonstrates that there is no significant difference in load capacity when the mesh sizes are 400 mm and 800 mm. If a mesh size of 200 mm is considered, a lower load capacity than 400 mm is expected (about 7 % less). However, a finer mesh caused a significant increase in computational costs, so the mesh size is selected between 400 mm and 800 mm. The number of elements used during mesh discretization varies from section to section until a good trade-off is reached between output accuracy and computational cost.

6.5. *Development of cracks under combined scour and traffic load*

Knowledge of trend in crack opening under different loading con-

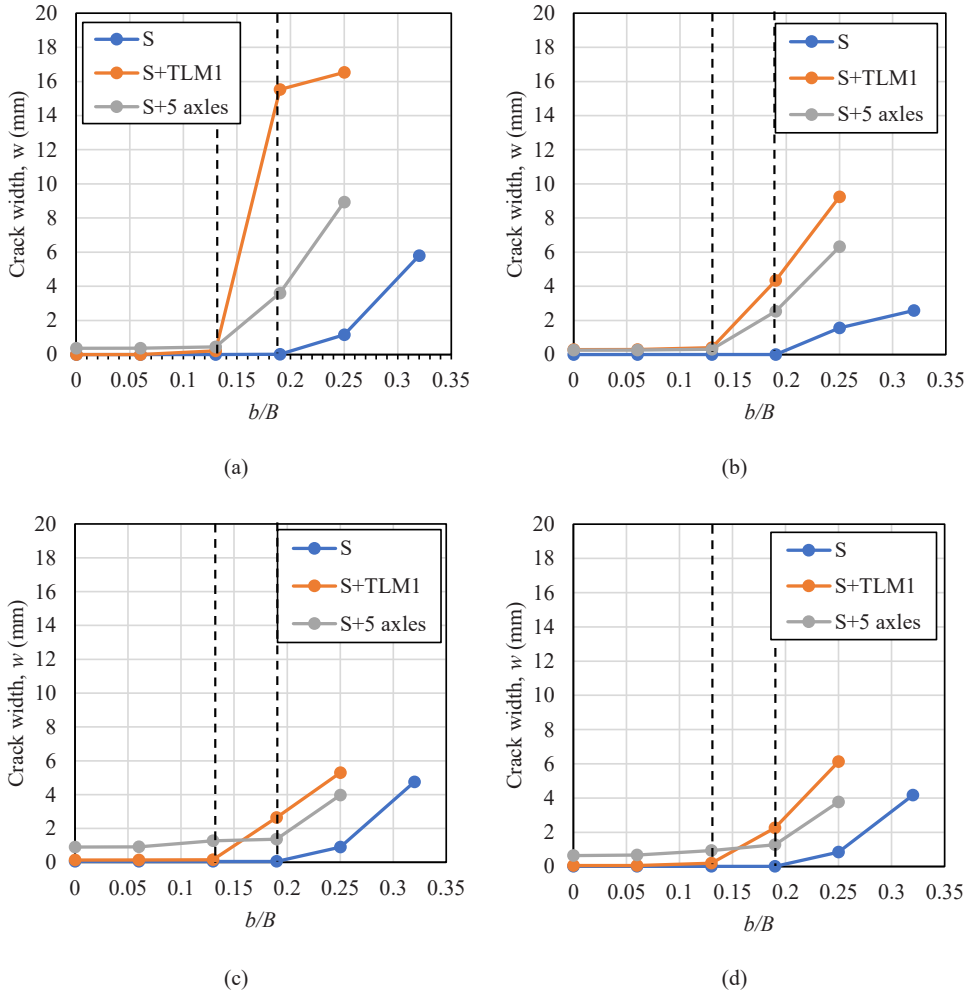

Fig. 26. Crack widths (w) recorded at (a) F1, (b) P1, (c) A1, and (d) A2 under increasing b/B.

ditions could be very useful for bridge monitoring and decision-making [21]. Demir and Caglar [55] proposed the following closed-form equation to estimate the crack width w when using the CDP model for describing the behavior of brittle materials:

$$w = \left[\varepsilon_t^{pl} + \frac{\sigma_t d_t}{(1-d_t)E_0}\right] l_w \tag{1}$$

where: $\varepsilon_t^{pl}$is the principal tensile plastic strain obtained from a FEM; $\sigma_t$is the tensile stress corresponding to ε_t^{pl};$d_t$is the damage parameter in tension; and $l_w$is the width of the fracture process zone (representative length) for the element of interest in the FE model.

If tensile damage is ignored in an FE analysis, ε_t^{pl} becomes equal to average fracture (inelastic) strain (ε_t^{ck}) and Eq. (1) can be simplified as;

$$w = \varepsilon_t^{ck} l_w \tag{2}$$

According to the proposed approach, the crack width at an element can be calculated by reading the principal tensile strain values at the desired step of the FE analyses and multiplying this by l_w. It is noteworthy that the mesh of the model is unstructured, although the aspect ratio is controlled by avoiding elements with very different lengths along the various directions. Thus, this approach is expected to provide only a rough estimate of crack widths. The values of l_w considered for calculating the crack width at the foundation (F1), pier (P1), and arch (A1 and A2) are equal to 580 mm, 420 mm and 490 mm respectively, and they correspond to the dimension of the element along the direction of cracking.

The crack width evolution at the selected sections of the bridge under increasing b/B is outlined in Fig. 26a through to d. Based on reported values of w, any inspection of cracked portions of the bridge requiring a measurement of crack width at different locations can suggest the level of scour at the foundation level. It can be seen that the combined influence of scour and LM1 leads to the formation of maximum crack width in all different sections of the bridge, followed by the case where scour is combined with 5-axles TLM. The least development of crack width is shown under scour only, namely, when traffic load is not considered: in this case $w < 1$ mm up to $b/B = 0.19$ and very limited cracking at the arch sections is observed up to $b/B = 0.25$. In the case of 5-axles TLM, small cracks ($w < 1$ mm) are formed under gravity load only at sections A1 and A2. Assuming that heavy vehicles are passing on the bridge (i.e., GVW = 440 kN), a crack width measured at P1 and F1 of the order of 2 mm could be representative of a scour level b/B approaching 20 %. In this case the managing agency could impose restrictions to heavier vehicles (e.g., GVW < 440 kN) in order to prevent severe damage or even collapse to the bridge.

7. Conclusions

In this study, a framework for multi-hazard structural assessment of roadway masonry arch bridges subjected to scour and traffic loading has been presented. For this purpose, a detailed 3D numerical model of a representative bridge structure has been developed, with the effect of scour modelled by progressively removing cohesive elements under the foundation. Various traffic load models have been considered to account

for different traffic load conditions according to both Eurocode 1 and the recent Italian guidelines for existing bridges. The structural performance and residual load-bearing capacity of the analysed bridge have been assessed at both local and global scales against traffic, scour and several combinations of these actions.

Based on the analysis results, the following main conclusions can be drawn:

- The analysis of the bridge subjected to gravity loads and scour results in significant levels of plastic deformations observed in many bridge components under $b/B = 0.31$ (corresponding to 31 % of foundation length being undermined by scour), corresponding to a collapse condition.
- Load-bearing capacity against traffic loading remains essentially equal to the that associated with no-scour conditions under scour levels b/B up to 0.13. However, a sudden drop in capacity is observed under higher levels of scour. Under $b/B = 0.19$, the residual traffic load capacity is 20 % of that related to the undamaged structure, whereas a total loss of capacity against traffic loading is attained under $b/B = 0.25$.
- The traffic load model has a significant influence on the load-carrying capacity in both the unscoured and scoured cases. Specifically, load factor α, which is the factor of the predicted load capacity over the total axles load of the selected traffic load model, progressively increases from LM1 to 5-axles TLM, 3-axles TLM, and 2-axles TLM under any scour level. The minimum value of load factor between those related to different TLMs might be used as a robustness measure of the bridge in engineering practice.
- The position of the TLM on top of the scoured pier produced the highest rate of decrease in load capacity, resulting into the lowest capacity under $b/B = 0.19$.
- The largest displacements recorded at the monitored locations are found under scour combined with tandem axle load, the lowest in case of scour combined with 5-axle load.

Furthermore, given the high level of uncertainty in material properties of masonry arch bridges, a sensitivity analysis has been carried out to investigate the impact of few critical ones on the bridge load capacity. It was found that higher values of tensile strength, fracture energy of masonry, and backfill cohesion all contribute to increase the capacity for the case of no scour but have also an impact on the reduction of capacity with scour. Thus, an accurate estimation of these properties or an adequate treatment of the uncertainty in these properties is essential in order to achieve confident estimates of the residual bridge capacity. A simplified crack opening formulation has been adopted to provide some predictions on the level of crack opening under different loading conditions and scour levels.

The output of this study is expected to support the assessment and management of masonry arch bridges subjected to traffic loading and scour hazard, and to allow decision-makers to be more aware of the scour levels that can produce unsafe conditions, failure or even collapse. The conclusions presented here are based on a specific, though representative, bridge structure. To gain broader insights into key behaviours and trends that may apply to a wider range of cases, analysing additional case studies is essential. Future developments of this study might include the assessment of masonry arch bridges with varying geometric and mechanical properties (including material degradation), as well as the development of more detailed soil-foundation-structure interaction models.

CRediT authorship contribution statement

Daniele Losanno: Writing – review & editing, Validation, Methodology, Investigation, Formal analysis, Conceptualization. **Prateek Kumar Dhir:** Writing – original draft, Visualization, Software, Investigation, Formal analysis, Data curation. **Fulvio Parisi:** Writing – review & editing, Validation, Supervision, Resources, Project administration, Methodology, Investigation, Funding acquisition, Formal analysis, Conceptualization. **Enrico Tubaldi:** Writing – review & editing, Validation, Methodology, Investigation, Formal analysis, Conceptualization.

Declaration of Competing Interest

I hereby declare that, to the authors' knowledge, no conflicts of interest in terms of either financial or personal relationships undermine the objectivity, credibility and validity of the research findings presented in the manuscript.

Acknowledgements

This study was carried out in the framework of RESIST project "RobustnEss aSsessment and retrofItting of bridgeS to prevenT progressive collapse under multiple hazards", which is funded by University of Naples Federico II and Compagnia di San Paolo through STAR Plus Programme 2020. Dr. Tubaldi gratefully acknowledges funding from the EPSRC-funded Innovation Launchpad Network+ (ILN+) Researcher in Residence (RiR) project "Improved models for the impact of floods on transport infrastructure assets" at Connected Places Catapult, London, UK (RIR23230615-8).

Data availability

Data will be made available on request.

References

[1] Koks EE, Rozenberg J, Zorn C, Tariverdi M, Vousdoukas M, Fraser SA, et al. A global multi-hazard risk analysis of road and railway infrastructure assets. Nat Commun 2019;10(1):2677.
[2] Sasidharan M, Parlikad AK, Schooling J, Hadjidemetriou GM, Hamer M, Kirwan A, et al. A bridge scour risk management approach to deal with uncertain climate future. Transp Res Part D: Transp Environ 2023;114:103567.
[3] Dikanski H, Imam B, Hagen-Zanker A. Effects of uncertain asset stock data on the assessment of climate change risks: a case study of bridge scour in the UK. Struct Saf 2018;71:1–12.
[4] Nasr A, Kjellström E, Björnsson I, Honfi D, Ivanov OL, Johansson J. Bridges in a changing climate: a study of the potential impacts of climate change on bridges and their possible adaptations. Struct Infrastruct Eng 2020;16(4):738–49.
[5] Nasr A, Björnsson I, Honfi D, Larsson Ivanov O, Johansson J, Kjellström E. A review of the potential impacts of climate change on the safety and performance of bridges. Sustain Resilient Infrastruct 2021;6(3-4):192–212.
[6] Ministero dei Trasporti. Consiglio Superiore dei Lavori Pubblici, "Linee guida per la classificazione e gestione del rischio, la valutazione della sicurezza ed il monitoraggio dei ponti esistenti,"; 2020.
[7] Nuti C, Briseghella B, Chen A, Lavorato D, Iori T, Vanzi I. Relevant outcomes from the history of Polcevera Viaduct in Genova, from design to nowadays failure. J Civ Struct Health Monit 2020;10:87–107.
[8] Cosenza E, Losanno D. Assessment of existing reinforced-concrete bridges under road-traffic loads according to the new Italian guidelines. Struct Concr 2021;22(5):2868–81.
[9] Page J. Masonry arch bridges: state-of-the-art review, transport research laboratory. HM Stationery Office; 1993.
[10] Tubaldi E, White CJ, Patelli E, Mitoulis S, De Almeida G, Brown J, et al. Invited perspectives: challenges and future directions in improving bridge flood resilience. Nat Hazards Earth Syst Sci Discuss 2021;2021:1–21.
[11] Tubaldi E, Macorini L, Izzuddin BA. Three-dimensional mesoscale modelling of multi-span masonry arch bridges subjected to scour. Eng Struct 2018;165:486–500.
[12] Zhang Y, Tubaldi E, Macorini L, Izzuddin BA. Mesoscale partitioned modelling of masonry bridges allowing for arch-backfill interaction. Constr Build Mater 2018;173:820–42.
[13] Milani G, Lourenço PB. 3D non-linear behavior of masonry arch bridges. Comput Struct 2012;110:133–50.
[14] Liu B, Sarhosis V, Lemos JV. Quantification of the crack propagation and global failure mechanism of single-and multi-ring masonry arch bridges. Eng Struct 2024;306:117805.
[15] Sobczyk B, Pyrzowski Ł, Miśkiewicz M. Computational modelling of historic masonry railroad arch bridges. Comput Struct 2024;291:107214.
[16] Zani G, Martinelli P, Galli A, di Prisco M. Three-dimensional modelling of a multi-span masonry arch bridge: influence of soil compressibility on the structural response under vertical static loads. Eng Struct 2020;221:110998.
[17] Borlenghi P, Saisi A, Gentile C. ND testing and establishing models of a multi-span masonry arch bridge. J Civ Struct Health Monit 2023;13(8):1595–611.

[18] Pantò B, Ortega J, Grosman S, Oliveira DV, Lourenço PB, Macorini L, et al. Advanced calibration of a 3D masonry arch bridge model using non-destructive testing and numerical optimisation. Constr Build Mater 2024;438:137131.
[19] Galassi S, Zampieri P. A new automatic procedure for nonlinear analysis of masonry arches subjected to large support movements. Eng Struct 2023;276:115359.
[20] Di Marco F, Tetougueni CD, Zampieri P, Pellegrino C. Numerical analysis of masonry arch bridges subject to scour effect. In: Proceedings of the 1st conference of the european association on quality control of bridges and structures: EUROSTRUCT 2021 1. Springer International Publishing; 2021. p. 1335–42.
[21] Scozzese F, Tubaldi E, Dall'Asta A. Damage metrics for masonry bridges under scour scenarios. Eng Struct 2023;296:116914.
[22] Zampieri P, Zanini MA, Faleschini F, Hofer L, Pellegrino C. Failure analysis of masonry arch bridges subject to local pier scour. Eng Fail Anal 2017;79:371–84.
[23] Tubaldi E, Macorini L, Izzuddin B. Flood risk assessment of masonry arch bridges. In: Proceedings of the 2nd international conference on uncertainty quantification in computational sciences and engineering, UNCECOMP; 2017. p. 15–7.
[24] Tubaldi E, Macorini L, Izzuddin BA. Identification of critical mechanical parameters for advanced analysis of masonry arch bridges. Struct Infrastruct Eng 2020;16(2):328–45.
[25] Tubaldi E, Minga E, Macorini L, Izzuddin BA. Mesoscale analysis of multi-span masonry arch bridges. Eng Struct 2020;225:111137.
[26] Scozzese F, Ragni L, Tubaldi E, Gara F. Modal properties variation and collapse assessment of masonry arch bridges under scour action. Eng Struct 2019;199:109665.
[27] Putcha C, Dutta S, Rodriguez J. Risk priority number for bridge failures. Pract Period Struct Des Constr 2020;25(2):04020010.
[28] Adam JM, Parisi F, Sagaseta J, Lu X. Research and practice on progressive collapse and robustness of building structures in the 21st century. Eng Struct 2018;173:122–49.
[29] Caredda G, Porcu MC, Buitrago M, Bertolesi E, Adam JM. Analysing local failure scenarios to assess the robustness of steel truss-type bridges. Eng Struct 2022;262:114341.
[30] Buitrago M, Bertolesi E, Calderón PA, Adam JM. Robustness of steel truss bridges: laboratory testing of a full-scale 21-metre bridge span. Structures 2021;29:691–700 (Elsevier).
[31] Bontempi F. Elementary concepts of structural robustness of bridges and viaducts. J Civ Struct Health Monit 2019;9:703–17.
[32] Jiang H, Wang J, Chorzepa MG, Zhao J. Numerical investigation of progressive collapse of a multispan continuous bridge subjected to vessel collision. J Bridge Eng 2017;22(5):04017008.
[33] Ghali A, Tadros G. Bridge progressive collapse vulnerability. J Struct Eng 1997;123(2):227–31.
[34] Starossek U. Avoiding disproportionate collapse of major bridges. Struct Eng Int 2009;19(3):289–97.
[35] André J, Anghileri M, Belletti B, Biondini F, Caspeele R, Demonceau J-F, et al. Guidance on the design for structural robustness. Joint Research Centre (JRC). JRC Tech Rep 2024.
[36] CNR DT 214/2018. Guide to Design of Structures for Robustness. National Research Council of Italy (CNR), Rome, 2021.
[37] Shoghijavan M, Starossek U. Developing a robustness index for parallel load-bearing systems. Eng Struct 2021;244:112742.
[38] Fan BH, Wang SG, Chen BC. Robustness assessment framework for through tied-arch bridge considering tie-bar failure. J Bridge Eng 2022;27(5):04022028.
[39] Fiorillo G, Ghosn M. Structural redundancy, robustness, and disproportionate collapse analysis of highway bridge superstructures. J Struct Eng 2022;148(7):04022075.
[40] Chen Q, Wang H, Bhattacharya B, El-Tawil S, Agrawal AK, Wong W. Reliability-Based Framework for Structural Robustness Evaluation of Bridges. J Bridge Eng 2024;29(6):04024035.
[41] Martinelli P, Colombo M, di Prisco M. Robustness assessment of half-joint RC girder bridges. Eng Struct 2024;306:117712.
[42] Maroni A, Tubaldi E, Ferguson N, Tarantino A, McDonald H, Zonta D. Electromagnetic sensors for underwater scour monitoring. Sensors 2020;20(15):4096.
[43] Abaqus, Dassault Systèmes. Accessed: Aug. 24; 2023. [Online]. Available: https://www.3ds.com/products-services/simulia/products/abaqus/.
[44] Lee J, Fenves GL. Plastic-damage model for cyclic loading of concrete structures. J Eng Mech 1998;124(8):892–900.
[45] Lubliner J, Oliver J, Oller S, Onate E. A plastic-damage model for concrete. Int J Solids Struct 1989;25(3):299–326.
[46] Abaqus documentation, Abaqus user manual," Dassault Systèmes Simulia Corporation. Accessed: Aug. 24; 2023. [Online]. Available: https://www.3ds.com/products-services/simulia/products/abaqus/.
[47] Fanning PJ, Boothby TE, Roberts BJ. Longitudinal and transverse effects in masonry arch assessment. Constr Build Mater 2001;15(1):51–60.
[48] Minga E, Macorini L, Izzuddin B. Enhanced mesoscale partitioned modelling of heterogeneous masonry structures. Int J Numer Methods Eng 2018;113(13):1950–71.
[49] Tubaldi E, Antonopoulos C, Mitoulis SA, Argyroudis S, Gara F, Ragni L, et al. Field tests and numerical analysis of the effects of scour on a full-scale soil–foundation–structural system. J Civ Struct Health Monit 2023;13(8):1461–81.
[50] Grosman S, Bilbao AB, Macorini L, Izzuddin BA. Numerical modelling of three-dimensional masonry arch bridge structures. Proc Inst Civ Eng-Eng Comput Mech 2021;174(2):96–113.
[51] FEMA 356, "Prestandard and commentary for the seismic rehabilitation of buildings," Federal Emergency Management Agency: Washington, DC, USA; 2000.
[52] Gazetas G. Foundation vibrations. In: Foundation engineering handbook. Boston, MA: Springer US; 1991. p. 553–93.
[53] CEN EN1991-2, Eurocode 1: Actions on structures—Part 2: Traffic loads on bridges," Brussels; 2003.
[54] Miluccio G, Losanno D, Parisi F, Cosenza E. Fragility analysis of existing prestressed concrete bridges under traffic loads according to new Italian guidelines. Struct Concr 2023;24(1):1053–69.
[55] Demir A, Caglar N. Numerical determination of crack width for reinforced concrete deep beams. Comput Concr, Int J 2020;25(3):193–204.